Effects of magnetic particles diameter and particle spacing on Biomagnetic flow and heat transfer over a linear/nonlinear stretched cylinder in the presence of magnetic dipole

Article *in* Journal of Mechanics in Medicine and Biology · April 2023

DOI: 10.1142/S0219519423500367

CITATIONS
2

READS
37

4 authors:

Mohammad Ferdows
University of Dhaka
226 PUBLICATIONS **3,520** CITATIONS
SEE PROFILE

Md. Jahangir Alam
Comilla University
29 PUBLICATIONS **156** CITATIONS
SEE PROFILE

Md. Ghulam Murtaza Talukder
Comilla University
69 PUBLICATIONS **365** CITATIONS
SEE PROFILE

Efstratios Tzirtzilakis
University of Peloponnese
96 PUBLICATIONS **1,922** CITATIONS
SEE PROFILE

Journal of Mechanics in Medicine and Biology
Vol. 23, No. 5 (2023) 2350036 (25 pages)

DOI: 10.1142/S0219519423500367

World Scientific
www.worldscientific.com

EFFECTS OF MAGNETIC PARTICLES DIAMETER AND PARTICLE SPACING ON BIOMAGNETIC FLOW AND HEAT TRANSFER OVER A LINEAR/NONLINEAR STRETCHED CYLINDER IN THE PRESENCE OF MAGNETIC DIPOLE

M. FERDOWS*,§, JAHANGIR ALAM*, M. G. MURTAZA† and E. E. TZIRTZILAKIS‡

*Research Group of Fluid Flow Modeling and Simulation
Department of Applied Mathematics University of Dhaka
Dhaka-1000, Bangladesh

†Department of Mathematics
Comilla University, Cumilla-3506, Bangladesh

‡Fluid Mechanics and Turbomachinary Laboratory
Department of Mechanical Engineering
University of the Peloponnese, Tripoli, Greece
§ferdows@du.ac.bd; ferdowsmohammad@yahoo.com

Received 8 November 2022
Revised 22 January 2023
Accepted 24 March 2023
Published 19 June 2023

Magnetic particles are essential in materials science, biomedical, bioengineering, heat exchangers due to their exceptional thermal conductivity and unique properties. This work aims to model and analyze the biomagnetic fluid flow and heat transfer, namely the flow of blood with magnetic particles (Fe_3O_4) induced by stretching cylinder with linear and nonlinear stretching velocities. Additionally, this study investigates the impact of particles diameter and their spacing under the influence of ferrohydrodynamics (FHD) principle. The collection of partial differential equations is transformed using similarity transformations to produce the theoretically stated ordinary differential system. An efficient numerical technique, which is further based on common finite difference method with central differencing, a tridiagonal matrix manipulation and an iterative procedure are used to solve the problem numerically. The major goal of this extensive study is to enhance heat transformation under the influence of numerous parameters. There have been numerous displays of the velocity profile, temperature distribution, local skin friction factor and rate of heat transfer in terms of the appearing physical parameters. It is observed that variation in velocity and temperature distributions is the cause of increasing the ferromagnetic interaction parameter and the size of magnetic particles. The enhancement of particle diameter causes an increment in the skin friction while the rate of heat

§Corresponding author.

transfer declines. For verifying purposes, a comparison is also shown with previously published scientific work and found to possess suitable accuracy.

Keywords: Biomagnetic fluid dynamics (BFD); blood; magnetic particles; particles spacing; stretched cylinder; finite difference method.

1. Introduction

Based on the applied research and wide range of applications in biomedical engineering, the study of magnetic fluid has become a hot issue in the 21st century. Magnetic fluid offers numerous ways to ameliorate the performance of heat transmission in regular fluid as blood, water, oil, etc. According to Choi,[1] the thermal conductivity of base fluid boost up when nanoparticles were mixed, and more importantly fluid heat transfer rate as well as increased and such characteristics are useful to apply in industrial sectors. Among all class of nanoparticles, magnetic particles have advantages to get suspended with biological fluids easily and providing the best solutions for biomedical applications especially in drug delivery.[2] Compared to other fields in fluid dynamics, biomagnetic fluid dynamics (BFD) is a relatively recent field. The study of BFD has recently attracted the interest of scientists since it directly relates to diseases and disorders of the human body, where the influence of magnetic field is vigorously explored. Due to the hemoglobin molecule, a type of iron oxide carried by the red blood cells, blood is one of the prominent examples in BFD that can behave as a magnetic fluid. As a result in BFD mathematical model both the principles namely- magnetohydrodynamics (MHD) and ferrohydrodynamics (FHD) are employed. Fundamentally, the BFD model is composed of the FHD and MHD concepts with the fluids being electrically nonconducting and the body force being due to magnetizationpolarization force.[3–5]

Following the discovery in Ref. 1, the study of nanofluid, or fluid that has been mixed with nanoparticles, has recently become more fascinating. The study of boundary layer flow and heat transfer due to stretching cylinder was initially investigated by Crane[6] and Wang[7] extended Crane's initial investigation and discovered that for higher Reynolds number values, fluid velocity and temperature dropped. Using water as the base fluid and Cu as nanoparticles, Pandey *et al.*[8] suggested a two-dimensional flow model over a stretching cylinder under the impact of thermal radiation. They found that the velocity boundary layer declined with increasing nanoparticle volume fraction, and the authors of this model used nanoparticle volume fraction up to 6%. Later on, Singh *et al.*[9] examined the Cu–H_2O flow and heat transfer through a porous stretchable cylinder in the presence of nonuniform heat source, where the volume fraction of solid particles was taken 0–25%. They reveal that with improvement of Reynolds number, temperature-dependent internal heat, the rate of heat elevated. Ashorynejad *et al.*[10] investigated the steady MHD flow of water-based nanofluid flow and heat transfer over a stretchable cylinder where three different types of nanoparticles, Cu, Al_2O_3, Ag and TiO_2, are considered. Their results show that for nanoparticles volume fraction, drag force factor increased

while local Nusselt number decreased. Alhussain *et al.*[11] discussed the two-dimensional flow of blood-based hybrid nanofluid over an expanding surface in the presence of magnetic field. The outputs were determined by utilizing the homotopy analysis method. Recently, Ferdows *et al.*[12] reported an unsteady BFD model which involves with those of FHD and MHD over a stretching/shrinking cylinder in presence of magnetic dipole. Where blood considered as base fluid and $CoFe_2O_4$ as magnetic particles. In this work, they also presented a graphical representation of BFD, FHD and MHD. They found that blood-$CoFe_2O_4$ velocity are remarkably decreased for BFD case compare than those of MHD and FHD model, where for BFD case temperature profile enhanced significantly. In all those cases especially in BFD they found that a strong magnetic field plays a vital role. Where, Alam *et al.*[13] demonstrated a graphical comparison of pure blood and blood with those of magnetic particles (Fe_3O_4) for each BFD, MHD, and FHD cases. In that study, they shows that magnetic particles had great influenced when mixed with blood. After adding magnetic particles with blood, fluid velocity significantly reduced than pure blood and those results are more comprehensively found for BFD case rather than FHD and MHD. Zeeshan *et al.*[14] examined the boundary layer flow of nanofluid over a stretching cylinder in non-Darcian Forchheimer porous media in presence of prescribed heat flux and thermal radiation. Basha *et al.*[15] carried out a comprehensive analysis of blood flow over the plate, wedge and stagnation point. They found that blood velocity decreases for magnetic Prandtl number.

Reddy *et al.*[16] presented single-walled carbon nanotubes (SWCNT)-Ag/water-based MHD hybrid nanofluid flow and heat transfer inside a square cavity under the influence of magnetic field and thermal radiation. They observed that when silver nanoparticles added with base fluid up to the values of particles volume fraction 0.05, the rate of heat transfer appreciably influenced and its augment is about 6.2–10.4%. Using a finite difference scheme, Reddy *et al.*[17] discussed the impact of magnetic field and thermal radiation on entropy generation and flow and heat transfer of MWCNTs-water nanofluid inside a square enclosure which is isentropic lines and isotherms features. Sreedevi *et al.*[18] discussed and presented a numerical analysis of hybrid nanofluid flow where Ethylene glycol considered as base fluid and aluminum oxide, SWCNTs considered as nanoparticles inside a square cavity. In their investigation, authors observed that in case of SWCNTs particles, the rate of heat transfer of base fluid enhanced from 8.2% to 17.6% taking volume fraction 0.05; while for alumina nanoparticles its augments from 8.2% to 12.4%. Reddy *et al.*[19] has developed a mathematical model of two-dimensional, steady, laminar flow and heat transfer of nanofluid over a vertical cone in the presence of magnetic field, thermal radiation with subject to convective boundary condition. The resultant ODEs are finally numerically solved by finite element method. Recently, Reddy *et al.*[20] studied the thermal water-Al_2O_3/TiO_2hybrid nanofluid flow over a two-dimensional stretching surface under the impacts of suction, slip condition. Ali *et al.*[21] demonstrated the melting effect for fluctuating temperature with Cattaneo–Christove features on the water-based MHD aligned nanofluid flow of the leading edge by

utilizing the finite element method. They accomplished that the efficiency of thermal increases straightaway as thermal relaxation and thermophoresis parameter enhanced. Using Galerkin numerical technique, Ali *et al.*[22] investigated the combined effects of bio-convection and magnetic field on unsteady Sakiadis and Blasius boundary layer flow of the accretion leading edge. An unsteady MHD bio-convective stagnation point boundary layer flow over a wedge under thermal radiation and chemical reaction effect was examined by Ali *et al.*[23] using finite element technique. The impact of thermal stratification and thermal radiation on MHD micropolar nanofluid flow over a shrinking sheet with prescribed heat flux was presented by Ali *et al.*[24]

The aforementioned literature shows that during the past few years, different kinds of FHD and MHD fluid flow via stretching/shrinking cylinder have been examined, but researchers have not paid enough attention to analyze the biomagnetic fluid flow over a nonlinear stretching cylinder. According to the best of the author's knowledge, no research has been done on the flow of biomagnetic fluid including magnetic particles due to a nonlinear stretching cylinder under no-slip conditions. This study will shed light on the following topics:

(i) The characteristics of linear and nonlinear blood-Fe_3O_4 flow.
(ii) Blood-Fe_3O_4 flow over cylinders and flat plates exhibits different physical behaviors.
(iii) The function of magnetic particle size and spacing in flow and heat transfer.

Careful observation on available study reveals that to date no studies have investigated the blood-Fe_3O_4 under the influence of magnetic dipole over a stretching cylinder accounting the effects of particle size and spacing. The mathematical assumptions of particle size and particle spacing are very closely interrelated to describe the mechanism of biological fluid flow. Due to the aforementioned characteristics, we built the current model by referring to the study.[3–5,25–28] An efficient numerical technique has been applied to solve this problem which further consists of common finite difference method, a tridiagonal matrix manipulation, and an iterative procedure. The impacts of appearing physical nondimensional parameters such as magnetic particles volume fraction, particle size, ferromagnetic number, curvature parameter are demonstrated graphically by flow distribution, temperature distribution as well as those of the skin friction coefficient and the Nusselt number and discussed with their respective outcomes. It is hoped that this work will be beneficial to upcoming researchers who are looking into the nanofluid model and using it in areas such as medication delivery, cancer treatment, MRI, and other pertinent applications.

2. Mathematical Formulation

A laminar, two-dimensional, steady, incompressible, electrically nonconducting biomagnetic fluid (blood) flow with magnetic particles (Fe_3O_4 as spherical shape)

over a nonlinear stretching cylinder having radius R has been investigated. The physical configuration of fluid flow is displayed in Fig. 1 where the fluid is stretched with velocity $U_w = cx^n$, c is a positive constant while n corresponds to linear $(n = 1)$ and nonlinear $(n \neq 1)$ stretching cylinder along x-axis and r-axis is taken as radial direction, respectively. It is assumed that the temperature of cylinder's surface $T_w = T_c + T_0 x^{2n-1}$ where T_0 is reference temperature and T_c is ambient fluid temperature with $T_w < T_c$. It is also supposed that a magnetic dipole is produced at center of x-axis by maintaining distance d from the surface which propagates a magnetic field of strength H.

After implementing the above assumptions, the governing continuity, momentum and energy equations take the form[3–5,12,13,27,28]

$$\frac{\partial}{\partial x}(ru) + \frac{\partial}{\partial r}(rv) = 0, \tag{1}$$

$$\rho_{mf}\left(u\frac{\partial u}{\partial x} + v\frac{\partial u}{\partial r}\right) = \mu_{mf}\left(\frac{1}{r}\frac{\partial u}{\partial r} + v\frac{\partial^2 u}{\partial r^2}\right) + \mu_0 M\frac{\partial H}{\partial x}, \tag{2}$$

$$(\rho C_p)_{mf}\left(u\frac{\partial T}{\partial x} + v\frac{\partial T}{\partial r}\right) + \mu_0 T\frac{\partial M}{\partial T}\left(u\frac{\partial H}{\partial x} + v\frac{\partial H}{\partial r}\right)$$

$$= \kappa_{mf}\left(\frac{\partial^2 T}{\partial r^2} + \frac{1}{r}\frac{\partial T}{\partial r}\right) + \mu_{mf}\left(\frac{\partial u}{\partial r}\right)^2 \tag{3}$$

with applicable boundary conditions

$$\begin{aligned} &r = R : u = U_w = cx^n, \quad v = 0, \quad T = T_w = T_c + T_0 x^{2n-1}, \\ &r \to \infty : u \to 0, \quad T \to T_c, \end{aligned} \tag{4}$$

where u and v denote the velocity components along x-axis and r-axis, respectively. In the above expression ρ is the biomagnetic fluid density, C_p is the specific heat at

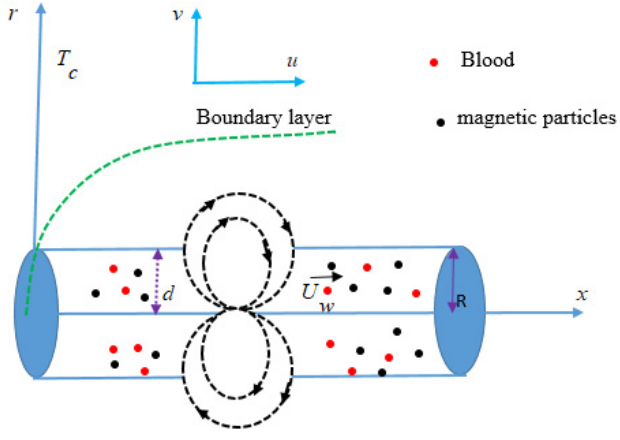

Fig. 1. Schematic diagram.

constant pressure, M is the magnetization, κ is the thermal conductivity, μ_0 is the magnetic permeability and μ is the dynamic viscosity.

The term $\mu_0 M \frac{\partial H}{\partial x}$ in momentum equation (2) represents the magnetic body force per unit volume while the second term $\mu_0 T \frac{\partial M}{\partial T}\left(u \frac{\partial H}{\partial x} + v \frac{\partial H}{\partial r}\right)$ on the right-hand side of energy equation (3) accounts for heating due to adiabatic magnetization. These two terms arise due to FHD.[3–5,29]

Following the studies,[3–5] the components of the magnetic field intensity H along x- and r-direction is given by

$$H_x(x,r) = -\frac{\gamma}{2\pi}\frac{x+d}{(x^2+(r+d)^2)} \quad \text{and} \quad H_r(x,r) = \frac{\gamma}{2\pi}\frac{x}{(x^2+(r+d)^2)}, \tag{5}$$

where γ is the magnetic field strength at the source point.

After calculating, the magnitude of the magnetic field intensity H is written as

$$H(x,r) = \sqrt{H_x^2 + H_r^2} = \frac{\gamma}{2\pi}\frac{1}{\sqrt{x^2+(r+d)^2}} = \frac{\gamma}{2\pi}\left[\frac{1}{(r+d)^2} - \frac{x^2}{2(r+d)^4}\right]. \tag{6}$$

According to Ref. 30, the magnetization M varies with temperature T and follows the mathematical relation

$$M = K(T_c - T), \tag{7}$$

where the pyromagnetic coefficient denoted by K and T_c is the Curie temperature.

To solve Eqs. (2) and (3) subject to the boundary conditions (4), the following similarity transformations have been introduced[28]:

$$\eta = \frac{r^2 - R^2}{2R}\left(\frac{c}{v_f}\right)^{1/2} x^{\frac{n-1}{2}}; \quad \psi = (cv_f)^{1/2} x^{\frac{n+1}{2}} R f(\eta); \quad \theta(\eta) = \frac{T_c - T}{T_c - T_w}, \tag{8}$$

where η and ψ is the similarity variable and stream function, respectively. The continuity equation (1) is automatically satisfied when the stream function is defined by $u = \frac{1}{r}\frac{\partial \psi}{\partial r}$ and $v = -\frac{1}{r}\frac{\partial \psi}{\partial x}$.

After implementing Eqs. (6)–(8) and with the help of Table 1, the governing equations (2) and (3) will take the following form:

$$A_1(1+2\eta D)f''' + \left(2A_1 D + A_2\left(\frac{n+1}{2}\right)f\right)f'' - A_2 n f'^2 - \frac{2\beta\theta}{(\eta+\alpha)^4} = 0, \tag{9}$$

$$(1+2\eta D)\theta'' + \left(2D + A_3 A_4 \mathrm{Pr}\left(\frac{n+1}{2}\right)f\right)\theta' + A_1 A_3 (1+2\eta D)\mathrm{Ec} f''^2 + 2A_3\beta\mathrm{Ec}(\varepsilon - \theta)\left[\frac{f'}{(\eta+\alpha)^4} + \frac{(n+1)f}{(\eta+\alpha)^5}\right] = 0, \tag{10}$$

Table 1. Thermophysical aspects of magnetic fluid.[25,28]

Thermophysical characteristics	Applied model
Dynamic viscosity	$\frac{\mu_{mf}}{\mu_f} = 1 + 2.5\varphi + 4.5\left[\frac{1}{\frac{h}{D_p}\left(2+\frac{h}{D_p}\right)\left(1+\frac{h}{D_p}\right)^2}\right]$
Density	$\rho_{mf} = (1-\varphi)\rho_f + \varphi\rho_s$
Heat capacity	$(\rho C_p)_{mf} = (1-\varphi)(\rho C_p)_f + \varphi(\rho C_p)_s$
Thermal conductivity	$\frac{\kappa_{mf}}{\kappa_f} = \frac{(\kappa_s+(m+1)\kappa_f)-(m-1)\varphi(\kappa_f-\kappa_s)}{(\kappa_s+(m-1)\kappa_f)+\varphi(\kappa_f-\kappa_s)}$

subject to the boundary conditions:

$$\begin{aligned} &f(0) = 0, \quad f'(0) = 1, \quad \theta(0) = 1, \\ &f'(\eta) \to 0, \quad \theta(\eta) \to 0, \quad \text{as } \eta \to \infty. \end{aligned} \tag{11}$$

Here,

$$A_1 = 1 + 2.5\varphi + 4.5\left[\frac{1}{\frac{h}{D_p}\left(2+\frac{h}{D_p}\right)\left(1+\frac{h}{D_p}\right)^2}\right],$$

$$A_2 = 1 - \varphi + \varphi\frac{\rho_s}{\rho_f}; \quad A_3 = \frac{\kappa_f}{\kappa_{mf}}; \quad A_4 = 1 - \varphi + \varphi\frac{(\rho C_p)_s}{(\rho C_p)_f}.$$

In the above expressions, $\beta = \frac{\gamma}{2\pi}\frac{\mu_0 K(T_c - T_w)\rho_f}{\mu_f^2}$ is the ferromagnetic interaction parameter; $\mathrm{Ec} = \frac{\mu_f U_w^2}{\kappa_f(T_c - T_w)}$ is the Eckert parameter; $\varepsilon = \frac{T_c}{T_c - T_w}$ is the Curie temperature; $D = \left(\frac{v_f}{cR^2x^{n-1}}\right)$ is the curvature parameter; $\alpha = \left(\frac{cx^{n-1}}{v_f}d^2\right)^{1/2}$ is the dimensionless distance and $\mathrm{Pr} = \frac{(\mu C_p)f}{\kappa_f}$ is the Prandtl number.

In the above expression, φ is the magnetic particle volume fraction, m is the particle shape factor while in this study we considered $m = 3$ which indicates that particles are in spherical shape.[29] Additionally, the symbols D_p and h represent the diameter of the magnetic particles and spacing between the particles, respectively. The subscripts mf and S represent magnetic fluid and solid particles (magnetic particles), respectively.

3. Physical Quantities

The physical quantities of interest in this study are the skin friction coefficient C_f (surface drag) and the local Nusselt number Nu_x (rate of heat transfer) given by the following expression.[28] With the help of Eq. (8), the following relation yields

$$C_f = \frac{\tau_w}{\rho_f U_w^2} = \left[1 + 2.5\varphi + 4.5\left[\frac{1}{\frac{h}{D_p}\left(2+\frac{h}{D_p}\right)\left(2+\frac{h}{D_p}\right)^2}\right]\right] \tag{12}$$

$$\mathrm{Re}^{-1/2} f''(0) \quad \text{and} \quad \mathrm{Nu}_x = \frac{xq_w}{\kappa_f(T_c - T_w)},$$

where the symbols τ_w and q_w represent the surface shear stress and surface heat flux, respectively, and mathematically defined by

$$\tau_w = \mu_{mf}\left(\frac{\partial u}{\partial r}\right)_{r=R} \quad \text{and} \quad q_w = -\kappa_{mf}\left(\frac{\partial T}{\partial r}\right)_{r=R}. \tag{13}$$

In Eq. (12), $\mathrm{Re} = \frac{U_w x}{\nu_f}$ is the local Reynolds number.

4. Numerical Technique

To solve the highly nonlinear equations, several numerical approaches have been proposed by the researchers over the last few decades. In fluid dynamics, to get an exact solution of such type of boundary layer flow equations Kafoussias *et al.*[31] developed a new algorithm which mainly consists of three essential features:

(i) This technique is constituted with finite difference method with central differencing.
(ii) On a tridiagonal matrix manipulation.
(iii) Finally, on an iterative procedure.

According to Refs. 5 and 31, momentum Eq. (9) takes the form

$$A_1(1+2\eta D)f''' + \left(2A_1 D + A_2\left(\frac{n+1}{2}\right)f\right)f'' - A_2 n f'^2 = \frac{2\beta\theta}{(\eta+\alpha)^4}. \tag{14}$$

Now, let $g(x) = f'(\eta)$ and therefore, Eq. (14) can be converted as a second-order linear differential equation provided that $f(\eta)$ is assumed to be a known function.

In such case Eq. (14) takes the form

$$A_1(1+2\eta D)(f')'' + \left(2A_1 D + A_2\left(\frac{n+1}{2}\right)f\right)(f')' - (A_2 n f')f' = \frac{2\beta\theta}{(\eta+\alpha)^4}.$$

This can be written as

$$P(x)g''(x) + Q(x)g'(x) + R(x)g(x) = S(x), \tag{15}$$

where

$$P(x) = A_1(1+2\eta D), \quad Q(x) = \left(2A_1 D + A_2\left(\frac{n+1}{2}\right)f\right),$$
$$R(x) = -A_2 n f', \quad S(x) = \frac{2\beta\theta}{(\eta+\alpha)^4}.$$

Equation (15) is now solved by implementing a common finite difference scheme based on central differencing and a tridiagonal matrix manipulation. It is essential to give an initial guess for $f'(\eta)$ before starting the numerical procedure between $\eta = 0$ and $\eta = \eta_\infty (\eta \to \infty)$ so as to satisfy the boundary conditions (11). For that, we consider the following assumptions:

$$f'(\eta) = 1 - \frac{\eta}{\eta_\infty}, \quad \theta = 1 - \frac{\eta}{\eta_\infty}.$$

The distribution of $f(\eta)$ is gained by the form of integration $f'(\eta)$ curve. After that, consider$f$ and θ are known and demarcate a newish estimation for $f'(\eta)$, (f'_{new}) by solving the nonlinear Eq. (15) using the above method. Therefore, the distribution of $f(\eta)$ is updated by integrating the new $f'(\eta)$ curves. These new distributions f and f' are then used for new inputs and so on. In this process, Eq. (14) and consequently Eq. (9) are solved iteratively until convergence up to a small quantity ε_1 is attained.

Consider a similar algorithm, for energy equation (10). Therefore,

$$(1+2\eta D)\theta'' + \left(2D + A_3A_4\text{Pr}\left(\frac{n+1}{2}\right)f\right)\theta' - 2A_3\beta\text{Ec}\left[\frac{f'}{(\eta+\alpha)^4} + \frac{(n+1)f}{(\eta+\alpha)^5}\right]\theta$$
$$= -A_1A_3(1+2\eta D)\text{Ec}f''^2 - 2A_3\beta\text{Ec}\varepsilon\left[\frac{f'}{(\eta+\alpha)^4} + \frac{(n+1)f}{(\eta+\alpha)^5}\right]. \tag{16}$$

Again let, $g(x) = \theta(\eta)$ in Eq. (16) which is already a second-order linear differential equation, and therefore, we have

$$P(x)g''(x) + Q(x)g'(x) + R(x)g(x) = S(x), \tag{17}$$

where

$$P(x) = (1+2\eta D), \quad Q(x) = \left(2D + A_3A_4\text{Pr}\left(\frac{n+1}{2}\right)f\right),$$
$$R(x) = -2A_3\beta\text{Ec}\left[\frac{f'}{(\eta+\alpha)^4} + \frac{(n+1)f}{(\eta+\alpha)^5}\right],$$
$$S(x) = -A_1A_3(1+2\eta D)\text{Ec}f''^2 - 2A_3\beta\text{Ec}\varepsilon\left[\frac{f'}{(\eta+\alpha)^4} + \frac{(n+1)f}{(\eta+\alpha)^5}\right].$$

In this way the profile of θ is obtained until the required convergence up to a small quantity ε_1 is attained. This process is continuing until the trial convergence of the solution is attained. The outcome of numerical results is obtained in this study by applying $\eta_\infty = 5$ with step size $h = \Delta\eta = 0.01$ and this continued until the required convergence $\varepsilon_1 = 10^{-5}$ is attained.

To estimate the accuracy of our obtained results, an error analysis was performed and results are added in Table 2. For finding percentage error the following

Table 2. Comparison values of the skin friction coefficient $f''(0)$ and the rate of heat transfer $-\theta'(0)$ with[32] when $n = 1, \text{Ec} = \varphi = \beta = 0$ for various values of D, S, Pr.

			Present results		Bhattacharyya *et al.*[32]		Error percentage	
D	S	Pr	$f''(0)$	$-\theta'(0)$	$f''(0)$	$-\theta'(0)$	$f''(0)$	$-\theta'(0)$
0.1	2.6	0.5	2.08137	1.11307	2.1003107	1.1198103	0.90108	0.60191
0.2	2.6	0.5	2.05862	1.12641	2.0588875	1.1225730	0.01299	0.34180
0.3	2.6	0.5	2.00769	1.13308	2.00884406	1.1310071	0.05744	0.18327
0.1	2.5	0.5	1.99631	1.06581	1.996264396	1.0671973	0.00228	0.12999
0.1	2.7	0.5	2.23141	1.27501	2.2315383	1.2746036	0.00574	0.03188

form is considered:

$$\text{Error} = \left(\left| \frac{N_p - N_{\text{ref}}}{N_{\text{ref}}} \right| \right) \times 100,$$

where N_p indicates the present obtained numerical results and N_{ref} are the numerical results of using references such as Ref. 32.

5. Discussion of Findings

The numerical outcomes of the computational precision of Eqs. (9) and (10) along with boundary conditions (11) are presented graphically for velocity, temperature distributions as well as the skin friction coefficient and the rate of heat transfer. Since the model is known as biomagnetic fluid and the numerical results are obtained for blood, it is essential to put realistic values in numerical computation for the appearing physical parameters. For that, a survey related to this topic was covered and values assigned as summarized in Table 3. Additionally, the values of thermophysical properties of base fluid (blood) and magnetic particles (Fe_3O_4) are depicted in Table 4.

In the above numerical assumptions, human body temperature $T_w = 37°C$[4,5,37] and body Curie temperature $T_c = 41°C$ are taken into consideration. Herein, in all figures we set up a comparison between

(i) the flow over a cylinder ($D \neq 0$) in both linear ($n = 1$) and nonlinear ($n \neq 1$) cases,
(ii) the flow over a flat plate ($D = 0$) in both linear ($n = 1$) and nonlinear ($n \neq 1$) cases,

Table 3. Values of physical parameters were performed in the present analysis.

Physical parameters	Value	References
Ferromagnetic interaction parameter (β)	0, 5, 10	5, 13, 30, 33
linear/nonlinear parameter (n)	1, 2, 10	27, 28
Curvature parameter (D)	0, 1	12, 28
Eckert number (Ec)	0.0001, 0.01, 0.5	34
Dimensionless distance (α)	1	12, 13
Volume fraction (φ)	0.001, 0.05, 0.1, 0.2	12, 28, 35
Prandtl number (Pr)	21, 25	5, 13, 34, 36
Curie temperature (ε)	78.5	3–5, 12, 13
Diameter of magnetic particles (D_p)	0.5, 1.5, 2.5	25
Spacing between particles (h)	2	26

Table 4. Thermophysical properties of blood and Fe_3O_4.[12,33]

Thermoyhysical characteristics	C_p (jkg^{-1}K^{-1})	ρ (kgm^{-3})	κ (Wm^{-1}K^{-1})
Blood	3.9×10^3	1050	0.5
Fe_3O_4	670	5180	9.7

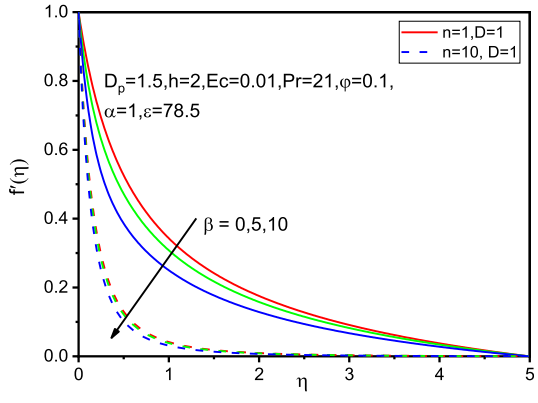

(a)

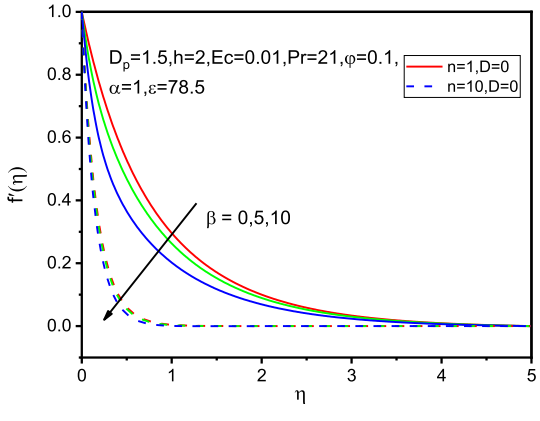

(b)

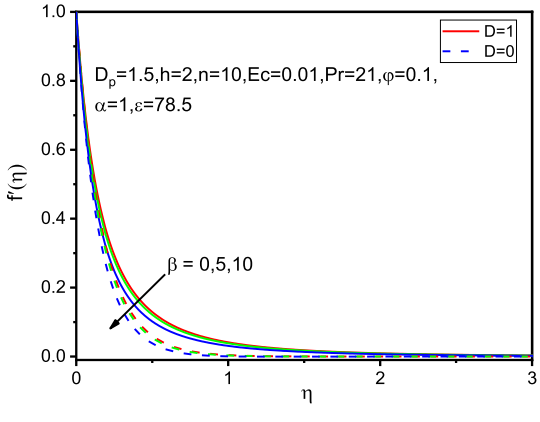

(c)

Fig. 2. Variation of β on velocity profile (a)–(c) and temperature profile (d)–(f) for different values of n and D.

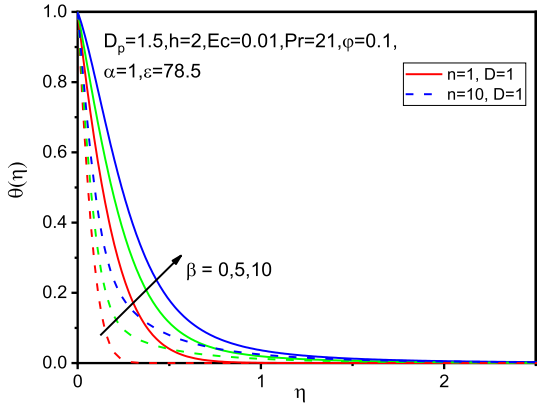

(d)

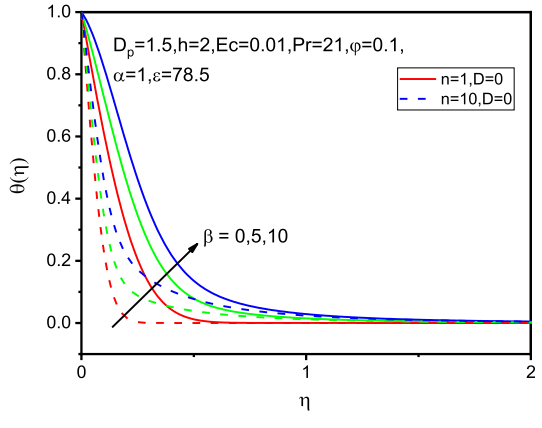

(e)

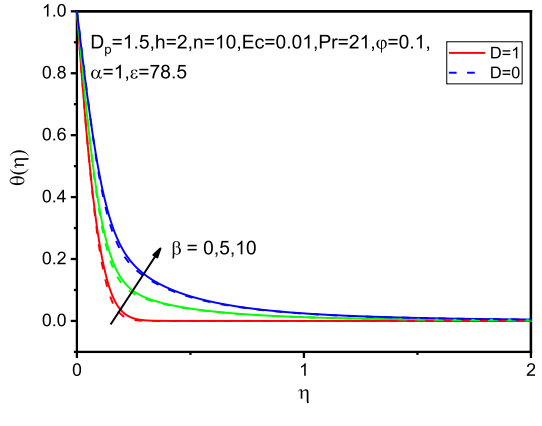

(f)

Fig. 2. (*Continued*)

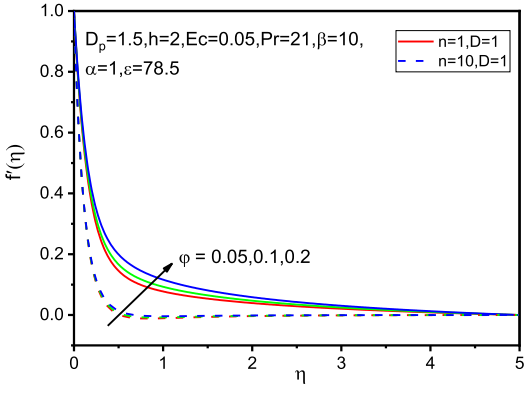

(a)

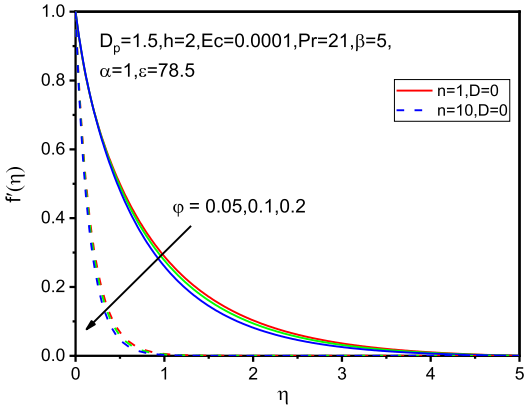

(b)

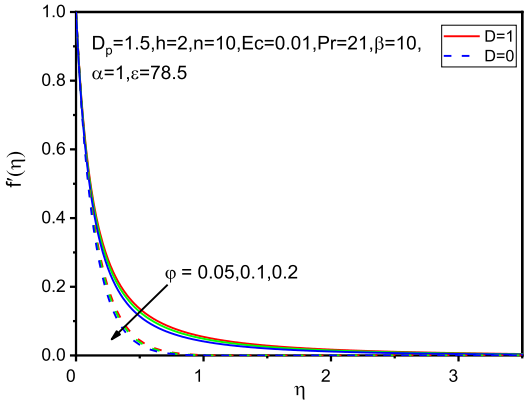

(c)

Fig. 3. Variation of φ on velocity profile (a)–(c) and temperature profile (d)–(f) for different values of n and D.

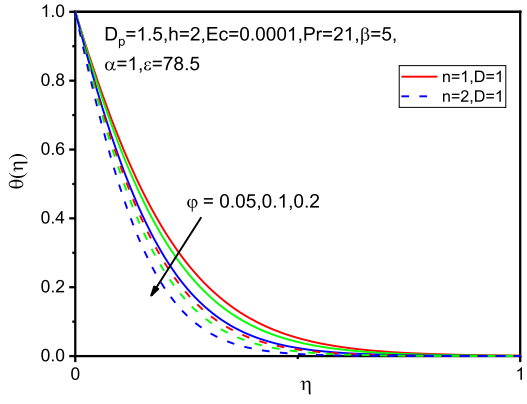

(d)

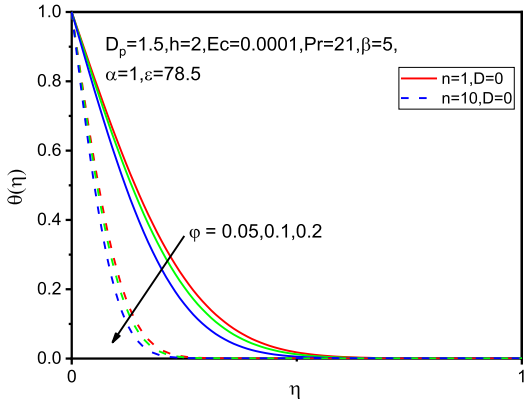

(e)

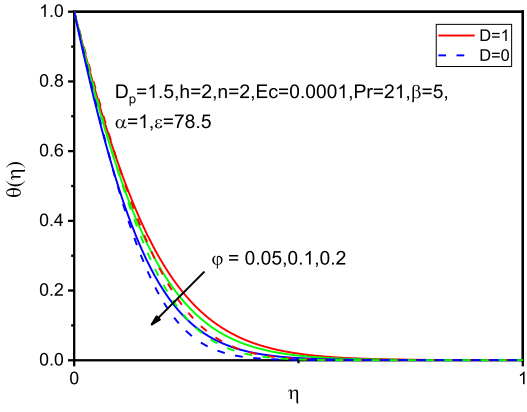

(f)

Fig. 3. (*Continued*)

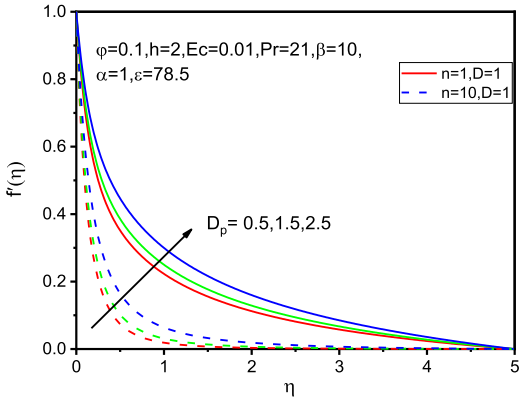

(a)

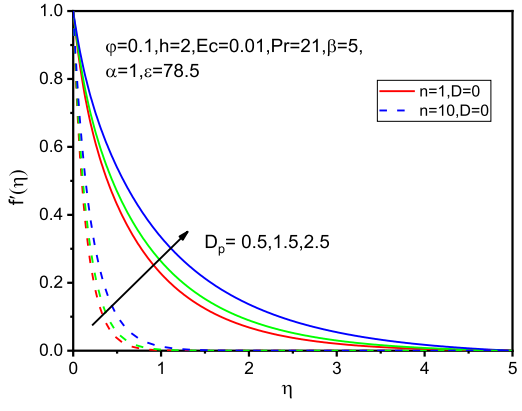

(b)

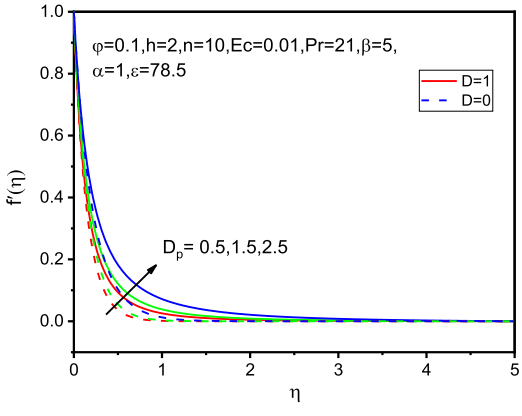

(c)

Fig. 4. Variation of D_p on velocity profile (a)–(c) and temperature profile (d)–(f) for different values of n and D.

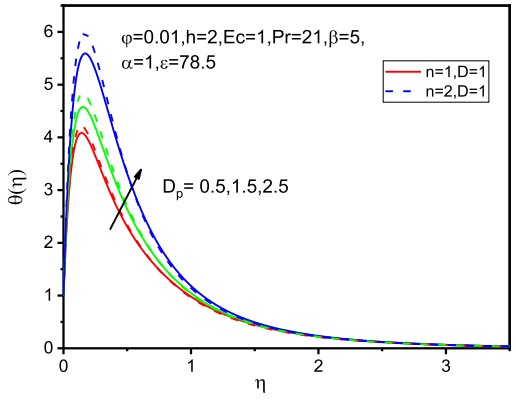

(d)

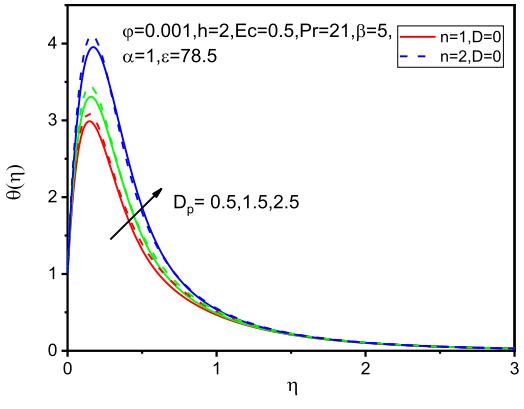

(e)

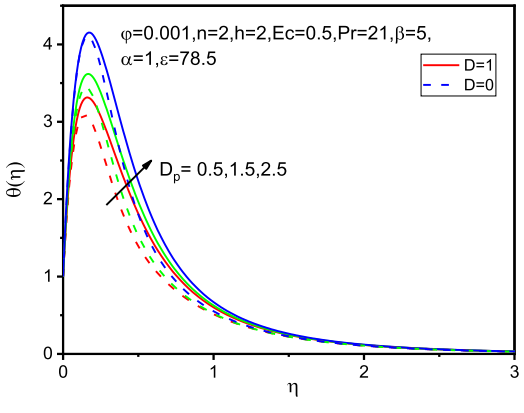

(f)

Fig. 4. (*Continued*)

(iii) the flow over a cylinder ($D \neq 0$) and flat plate ($D = 0$) for nonlinear ($n \neq 1$) case.

Figure 2 depicts the physical behavior of blood-Fe_3O_4 on velocity and temperature profiles for ferromagnetic interaction parameter β in terms of various values of n and D. Figure 2(a) exhibits the variation of β on velocity profile for the flow over cylinder in linear and nonlinear cases; whereas Fig. 2(b) exhibits for the flow over a flat plate. It is noticed from these figures that with the increasing values of β, blood-Fe_3O_4 velocity is decreased. By applying a strong magnetic field in the concerned boundary

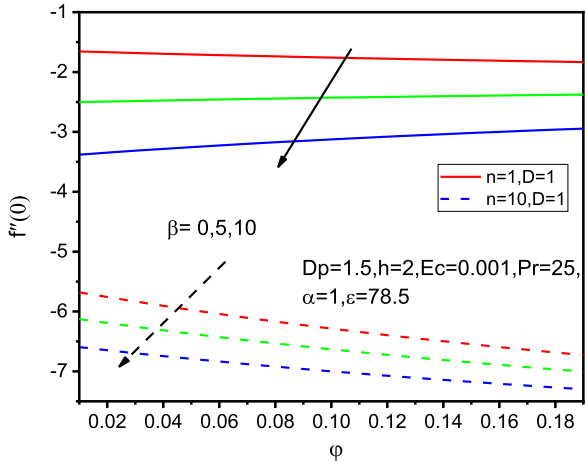

(a)

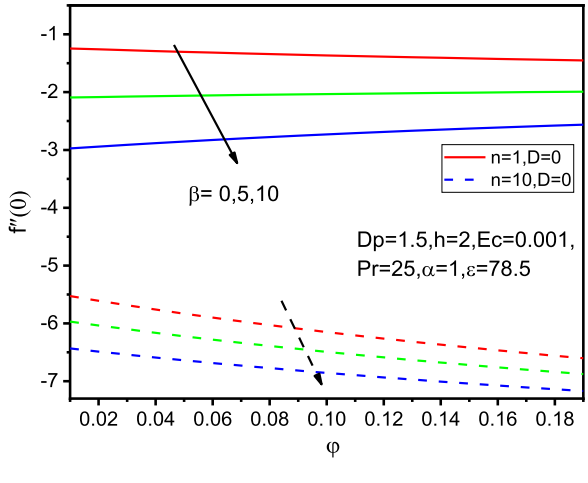

(b)

Fig. 5. Variation of θ on $f''(0)$ and $-\theta'(0)$ for various values of n and D with regard to φ.

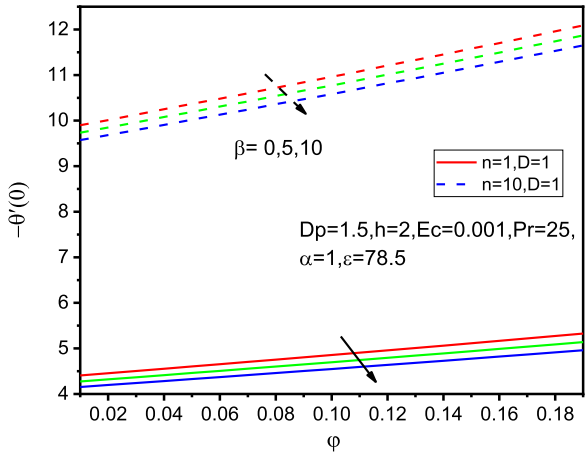

(c)

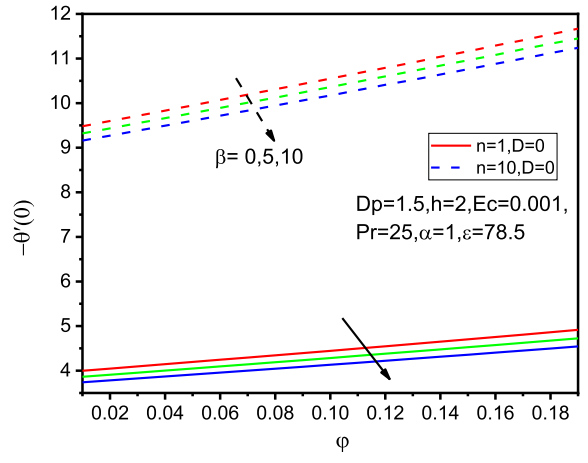

(d)

Fig. 5. (*Continued*)

layer region, a resisting force is produced known as Kelvin force and this force acts opposite to the direction of flow. Increase in β leads to decline in the fluid velocity. It can be also observed from these figures that fluid velocity is reduced remarkably in nonlinear case compared to that of linear case. However, Fig. 2(c) demonstrates only for nonlinear case with respect to both cylindrical surface and flow over a flat plate. In this case, it can be seen that for nonlinear case, fluid velocity is increased comprehensively when flowing over a cylinder rather than flat plate. The reverse trend is observed in the temperature distributions (see Figs. 2(d)–2(f)).

Figure 3 demonstrates the effects of the magnetic particles volume fraction φ on the velocity and temperature profiles for both linear and nonlinear cases in the

direction of flow along flat plate and cylinder. It is visible from these figures that fluid velocity is increased when flowing over cylinder in both linear and nonlinear cases (see Fig. 3(a)) but a reverse trend is observed in Fig. 3(b) with increase in the suspension of magnetic particles volume fraction on blood. While, Fig. 3(c) reveals that for nonlinear case, fluid velocity is significantly increased along cylinder compared to flat plate. Additionally, Figs. 3(d)–3(f) show the effect of φ on temperature distributions in different cases. All these figures illustrate this agreement with the physical behavior that when the values of φ enhanced gradually, the temperature remarkably increased in the cylinder case and it is more pronounced in linear case compared to the nonlinear case.

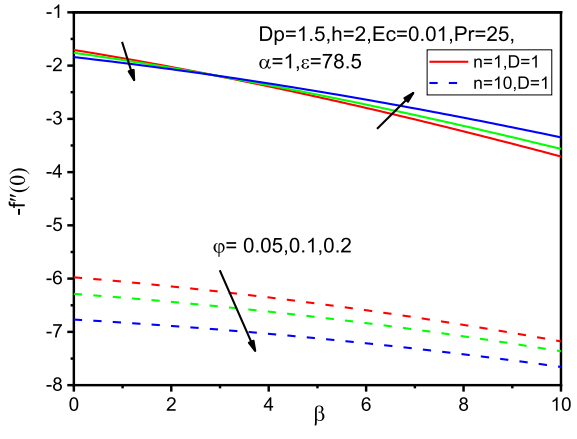

(a)

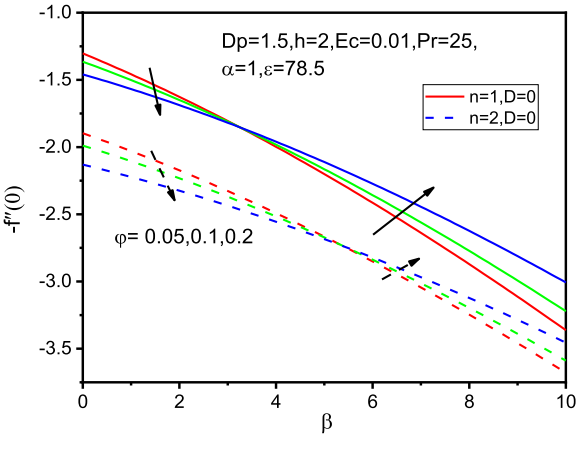

(b)

Fig. 6. Variation of φ on $f''(0)$ and $-\theta'(0)$ for various values of n and D with regard to β.

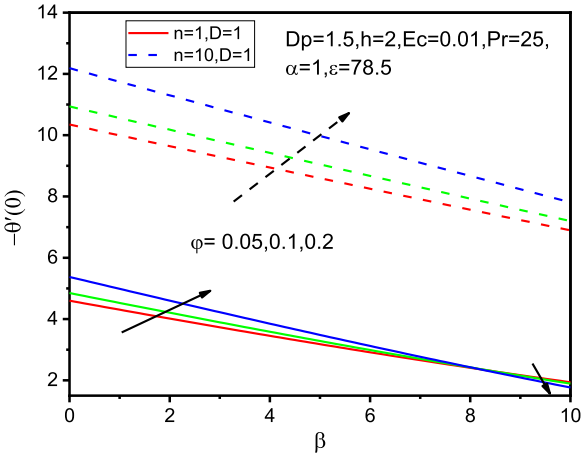

(c)

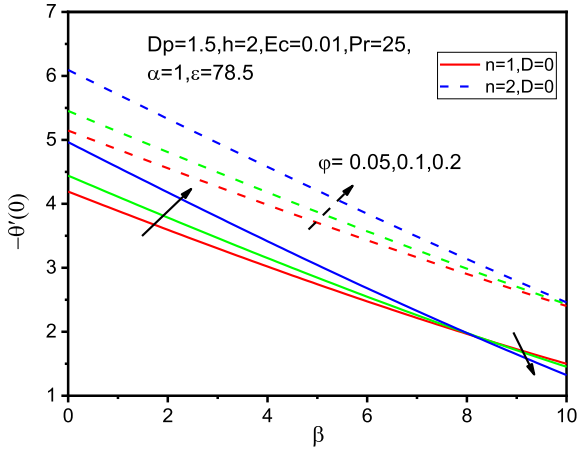

(d)

Fig. 6. (*Continued*)

The analysis of the effect of magnetic particle diameter when it suspends to the base fluid, such as blood, is the most crucial component of this work. The magnetic particle diameters used in this work range from 0.5 nm to 2.5 nm, with each particle spaced at a distance of 2 nm. The numerical results are shown in Figs. 4(a)–4(f). Here, it is deduced from all of these images that an increase in magnetic particle diameter leads to an increase in fluid velocity and temperature profiles. When the flow through a cylinder is treated as a linear case, the findings are more significant.

Finally, the variations of the skin friction coefficient and the Nusselt number for varying values of ferromagnetic interaction parameter, magnetic particles volume fraction and magnetic particles diameter have been expressed in Figs. 5–7. The

impact of ferromagnetic number on $f''(0)$ and $-\theta'(0)$ with regard to volume fraction φ is displayed in Figs. 5(a)–5(d). These figures exposed that both $f''(0)$ and $-\theta'(0)$ decline with augment values of φ and it is well found that the skin friction coefficient increased (see Figs. 5(a) and 5(b)) in linear case when flowing along cylinder but opposite trend is observed in $-\theta'(0)$ (see Figs. 5(c) and 5(d)) which expresses that the rate of heat transfer of fluid is more pronounced in nonlinear case over cylinder rather than flat plate.

Figure 6 exhibits the variation of $f''(0)$ and $-\theta'(0)$ for various values of φ with regard to β. The variations of magnetic particles are taken up to 20% in this study and two types of solutions on $f''(0)$ and $-\theta'(0)$ have been found. Figures 6(a)–6(d) show that for nonlinear case over cylinder $f''(0)$ is decreased while $-\theta'(0)$ is enhanced compared to the flat plate in the linear case.

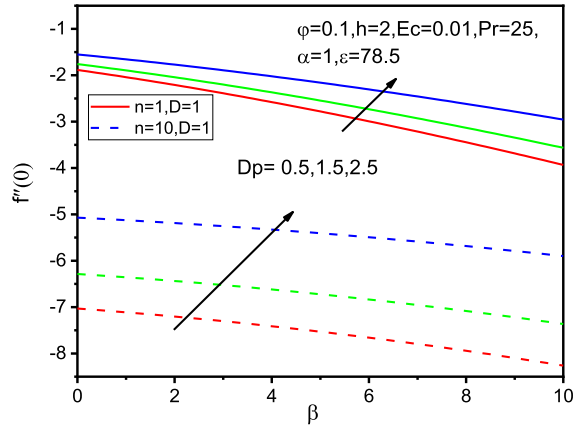

(a)

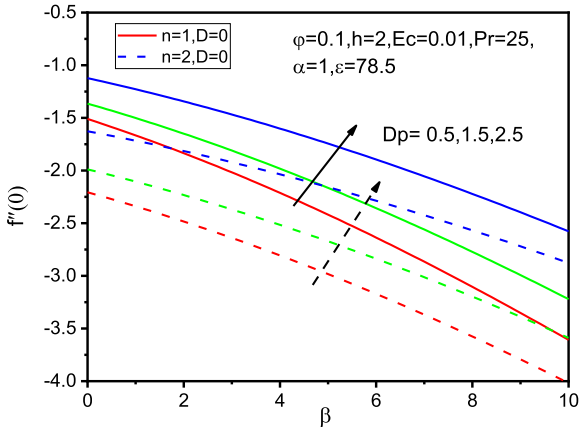

(b)

Fig. 7. Variation of D_p on $f''(0)$ and $-\theta'(0)$ for various values of n and D with regard to β.

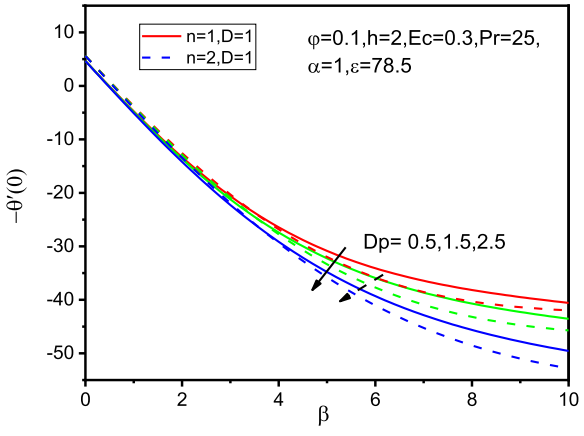

(c)

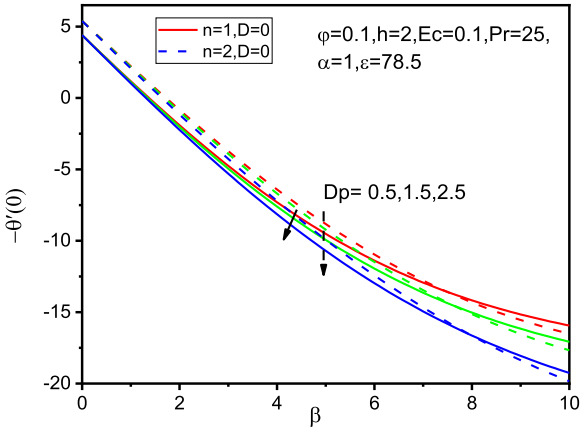

(d)

Fig. 7. (*Continued*)

The importance of D_p on $f''(0)$ and $-\theta'(0)$ was investigated and the outcomes of numerical results are shown in Figs. 7(a)–7(d). These figures reveal that, with rising values D_p, $f''(0)$ is increased; whereas a reverse trend is observed in $-\theta'(0)$. From Figs. 7(a) and 7(b), it is perceived that $f''(0)$ increased comprehensively in the linear case rather than in the nonlinear case.

6. Conclusions

In this study, a common finite difference numerical scheme is used to describe the flow and heat characteristics of blood-Fe_3O_4 under the influence of magnetic dipole over a stretching cylinder. The impacts of blooming physical parameters on

distributions of velocity, temperature, coefficient of skin friction and rate of heat transfer have been conceived. From the present investigation the following interesting observations can be drawn:

(i) A significant enhancement is observed on velocity and temperature distributions for linear case compared to nonlinear case and this is appreciable in cylindrical cases than in flat plate cases.
(ii) In nonlinear case both velocity and temperature are remarkably enhanced for cylindrical surface than that of flat surface.
(iii) Velocity profile declined for the boosting values of ferromagnetic interaction parameter.
(iv) With rising values of magnetic particles volume fraction, it has been observed that temperature profile decreased.
(v) The magnetic particle diameter is directly proportional to flow and temperature.
(vi) Both skin friction coefficient and rate of heat transfer showed decrease with the augmenting values of ferromagnetic number. The skin friction coefficient decreased significantly in the nonlinear cylindrical case whereas the reverse trend is found in the rate of heat transfer.
(vii) Enhancement of the rate of heat transfer can be done by increasing the values of magnetic particle volume fraction.
(viii) The magnetic particle diameter gives the highest value of skin friction coefficient in nonlinear case when flowing over cylinder compared to that of flat plate; while the rate of heat transfer provides the reverse results.

Acknowledgment

The authors also would like to thank the Bose Centre for Advanced Study and Research in Natural Sciences, University of Dhaka for their financial support.

References

1. Choi SUS, Eastman JA, Enhancing thermal conductivity of fluids with nanoparticles, *Proc ASME Int Mechanical Engineering Congress & Exposition*, San Francisco, CA, USA, pp. 99–105, 12–17 November 1995.
2. Kenjereš S, Tjin JL, Numerical simulations of targeted delivery of magnetic drug aerosols in the human upper and central respiratory system: A validation study, *R Soc Open Sci* **4**:170873, 2017, doi: 10.1098/rsos.170873.
3. Tzirtzilakis EE, A mathematical model for blood flow in magnetic field, *Phys Fluids* **17**(7):077103-1–077103-14, 2005.
4. Tzirtzilakis EE, Biomagnetic fluid flow in an aneurysm using ferrohydrodynamics principles, *Phys Fluids* **27**:061902, 2015.
5. Murtaza MG, Tzirtzilakis EE, Ferdows M, Effect of electrical conductivity and magnetization on the biomagnetic fluid flow over a stretching sheet, *Z Angew Math Phys* **68**:93, 2017.

6. Crane LJ, Boundary layer flow due to a stretching cylinder, *Z Angew Math Phys* **26**(5):619–622, 1975.
7. Wang CY, Fluid flow due to a stretching cylinder, *Phys Fluids* **31**(3):466–468, 1998.
8. Pandey AK, Kumar M, Boundary layer flow and heat transfer analysis on Cu–water nanofuid flow a stretching cylinder with slip, *Alex Eng J* **56**(4):671–677, 2017.
9. Sing K, Pandey AK, Kumar M, Melting heat transfer assessment on magnetic nanofuid fow past a porous stretching cylinder, *J Egypt Math Soc* **29**:1, 2021.
10. Ashorynejad HR, Sheikholeslami M, Po, I, Ganji DD, Nanofluid flow and heat transfer due to a stretching cylinder in the presence of magnetic field, *Heat Mass Transf* **49**:427–436, 2013.
11. Alhussain ZA, Tassaddiq A, Thin film blood based casson hybrid nanofuid flow with variable viscosity, *Arab J Sci Eng* **47**:1087–1094, 2022.
12. Ferdows M, Alam J, Murtaza G, Tzirtzilakis EE, Sun S, Biomagnetic flow with $CoFe_2O_4$ magnetic particles through an unsteady stretching/shrinking cylinder, *Magnetochemistry* **8**:27, 2022.
13. Alam J, Murtaza MG, Tzirtzilakis EE, Ferdows M, Magnetohydrodynamic and ferrohydrodynamic interactions on the biomagnetic flow and heat transfer containing magnetic particles along a stretched cylinder, *Eur J Comput Mech* **31**(1):1–40, 2022.
14. Zeeshan A, Maskeen MM, Mehmood OU, Hydromagnetic nanofluid flow past a stretching cylinder embedded in non-Darcian Forchheimer porous media, *Neural Comput Appl* **30**:3479–3489, 2018.
15. Basha HT, Sivaraj R, Numerical simulation of blood nanofluid flow over three different geometries by means of gyrotactic microorganisms: Applications to the flow in a circulatory system, *Proc Inst Mech Eng C: J Mech Eng Sci* **235**(2):441–460, 2021.
16. Reddy PS, Sreedevi P, Effect of thermal radiation on heat transfer and entropy generation analysis of MHD hybrid nanofluid inside a square cavity, *Waves Random Complex Media* **1**:1–33; 2022, doi: 10.1080/17455030.2021.2023780.
17. Reddy PS, Sreedevi P, Reddy VN, Entropy generation and heat transfer analysis of magnetic nanofluid flow inside a square cavity filled with carbon nanotubes, *Chem Thermodyn Therm Anal* **6**:10045, 2022.
18. Sreedevi P, Reddy PS, Entropy generation and heat transfer analysis of alumina and carbon nanotubes based hybrid nanofluid flow inside a cavity, *Phys Scr* **96**:085210, 2021.
19. Reddy PS, Sreedevi P, Chamkha AJ, Magnetohydrodynamic (MHD) boundary layer heat and mass transfer characteristics of nanofluid over a vertical cone under convective boundary condition, *Propuls Power Res* **7**(4):308–319, 2018.
20. Reddy PS, Sreedevi P, Chamkha AJ, Hybrid nanofluid heat and mass transfer characteristics over a stretching/shrinking sheet with slip effects, *J Nanofluids* **12**:251–260, 2023.
21. Ali L, Ali B, Ghori MB, Melting effect on Cattaneo–Christov and thermal radiation features for aligned MHD nanofluid flow comprising microorganism to leading edge: FEM approach, *Comput Math Appl* **109**:260–269, 2022.
22. Ali L, Ali B, Liu X, Ahmed S, Shah MA, Analysis of bio-convective MHD Blasius and Sakiadis flow with Cattaneo–Christov heat flux model and chemical reaction, *Chin J Phys* **77**:1963–1975, 2022.
23. Ali L, Ali B, Liu X, Iqbal T, Zulqarnain RM, Javid M, A comparative study of unsteady MHD Falkner-Skan wedge flow for non-Newtonian nanofluids considering thermal radiation and activation energy, *Chin J Phys* **77**:1625–1638, 2022.
24. Ali L, Ali B, Mousa AAA, Hammouch Z, Hussain S, Siddique I, Huang Y, Insight into significance of thermal stratification and radiation on dynamics of micropolar water based

TiO_2 nanoparticle via finite element simulation, *J Mater Res Technol* **19**:4209–4219, 2022.
25. Ali L, Wang Ye, Ali B, Liu X, Din A, Al Mdallal Q, The function of nanoparticle's diameter and Darcy–Forchheimer flow over a cylinder with effect of magnetic field and thermal radiation, *Case Studies Therm Eng* **28**:101392, 2021.
26. Gosukonda S, Srikantj Gorti VPN, Baluguri SB, Sakam SR, Particle spacing and chemical reaction effects on convective heat transfer through a nano-fluid in cylindrical annulus, *Procedia Eng* **127**:263–270, 2015.
27. Khan M, Malik R, Hussain M, Nonlinear radiative heat transfer to stagnation-point flow of Sisko fluid past a stretching cylinder, *AIP Adv* **6**:055315, 2016.
28. Kardri MA, Bachok N, Arifin NM, Ali FM, Rahim YF, Magnetohydrodynamic flow past a nonlinear stretching or shrinking cylinder in nanofluid with viscous dissipation and heat generation effect, *J Adv Res Fluid Mech Therm Sci* **90**(1):102–114, 2022.
29. Kandasamy R, Atikh bt Adnan N, Mohammad R, Nanoparticles shape effects on squeezed MHD flow of water based on Cu, Al_2O_3 and SWCNTs over a porous sensor surface, *Alex Eng J* **57**(3):1433–1445, 2018.
30. Murtaza MG, Tzirtzilakis EE, Ferdows M, Similarity solutions of nonlinear stretched biomagnetic flow and heat transfer with signum function and temperature power law geometries, *Int J Math Comput Sci* **12**:2, 2018.
31. Kafoussias NG, Williams EW, An improved approximation technique to obtain numerical solution of a class of two point boundary value similarity problems in fluid mechanics, *Int J Numer Methods Fluids* **17**:145–162, 1993.
32. Bhattacharyya K, Gorla RSR, Boundary layer flow and heat transfer over a permeable shrinking cylinder with surface mass transfer, *Int J Appl Mech Eng* **18**(4):1003–1012, 2013.
33. Alam J, Murtaza MG, Tzirtzilakis EE, Ferdows M, Application of biomagnetic fluid dynamics modelling for simulation of flow with magnetic particles and variable fluid properties over a stretching cylinder, *Math Comput Simul* **199**:438–462, 2022.
34. Hady FM, Mahdy A, Mohamed RA, Abo Zaid OA, Effects of viscous dissipation on unsteady MHD thermo bioconvection boundary layer flow of a nanofluid containing gyrotactic microorganisms along a stretching sheet, *World J Mech*, **6**:505–526, 2016.
35. Alam J, Murtaza G, Tzirtzilakis EE, Ferdows M, Effect of thermal radiation on biomagnetic fluid flow and heat transfer over an unsteady stretching sheet, *Comput Assist Methods Eng Sci* **28**:81–104, 2021.
36. Alam J, Murtaza MG, Tzirtzilakis EE, Ferdows M, Group method analysis for Blood-Mn-$ZnFe_2O_4$ flow and heat transfer under ferrohydrodynamics through a stretched cylinder, *Math Methods Appl Sci* **45**:11807–11827, 2022.
37. Tzirtzilakis EE, Xenos M, Loukopoulos VC, Kafoussias NG, Turbulent biomagnetic fluid flow in a rectangular channel under the action of a localized magnetic field, *Int J Eng Sci* **44**(18–19): 1205–1224, 2006.